Supporting Information for:

Poisoning effect of adsorbed CO during CO_2 electroreduction on late transition metals

Sneha A. Akhade[a], Wenjia Luo[b], Xiaowa Nie[b], Nicole J. Bernstein[a], Aravind Asthagiri[b], Michael J. Janik[a,*]

[a] Department of Chemical Engineering, Fenske Laboratory, Pennsylvania State University, State College, PA 16802
[b] Department of Chemical and Biomolecular Engineering, Koffolt Laboratories, Ohio State University, Columbus, OH 43210

* Corresponding author. Tel.: +1 814 863 9366; fax: +1 814 865 7846.
Email address: mjanik@psu.edu

TABLE OF CONTENTS

1. Potential dependent free energies $\Delta G[U]$ at low coverage, θ = 1/9th ML

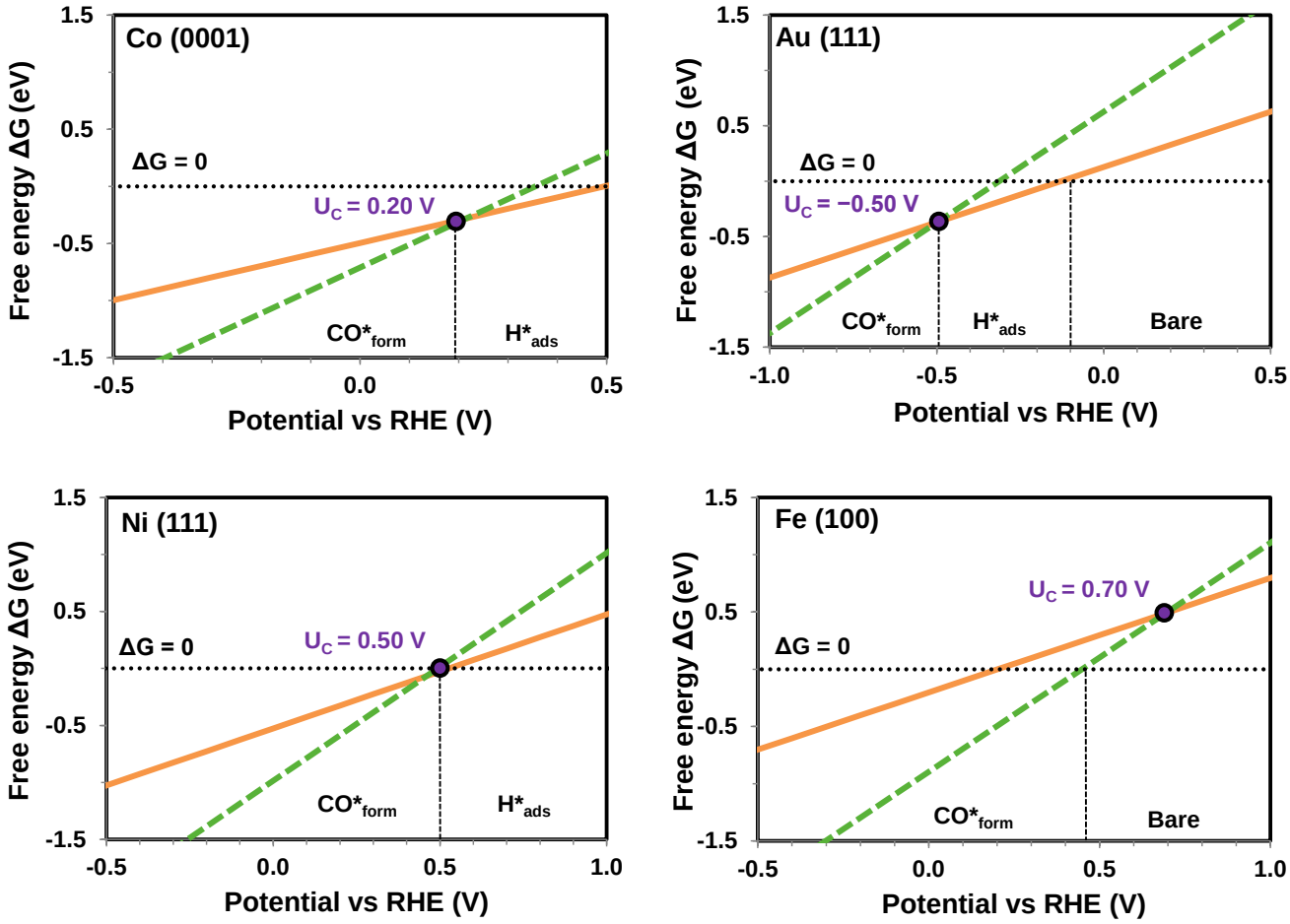

Figure S 1. Potential dependent free energies $\Delta G[U]$ of CO* formation (dashed - -) and H* adsorption (smooth –) at θ = 1/9th ML on metal surfaces during CO_2 ER. The dotted line (▪▪▪) represents the equilibrium condition $\Delta G[U^0] = 0$.

2. Potential dependent free energies $\Delta G[U]$ at high coverage, θ = 1 ML

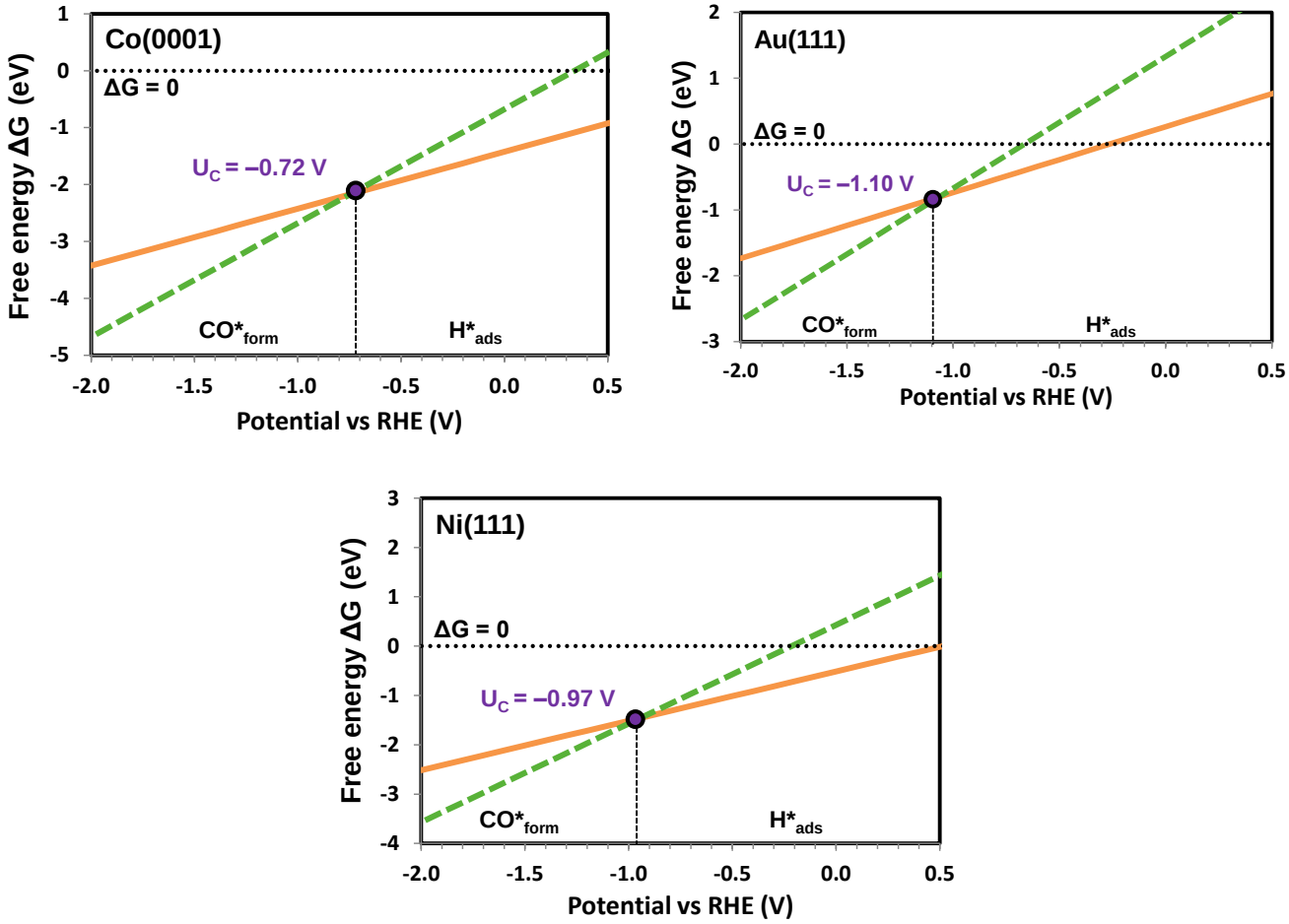

Figure S 2. Potential dependent free energies $\Delta G[U]$ of CO* formation (dashed - -) and H* adsorption (smooth –) at θ = 1 ML on metal surfaces during CO_2 ER. The dotted line (▪▪▪) represents the equilibrium condition $\Delta G[U^0] = 0$.

3. Surface coverage dependent free energies $\Delta G[\theta,U]$

Figure S3 below shows the coverage dependent reaction free energies for CO* and H* formation on all five metal surfaces considered, at $U = -0.5$ V-RHE. The free energy of CO* formation ($\Delta G_{rxn}^{CO^*}[\theta]$) is more sensitive to surface coverage than that of H* adsorption ($\Delta G_{ads}^{\mathrm{H}^*}[\theta]$). Thus, a third-order polynomial fit is employed to describe the continuous coverage dependence of CO* formation. A linear fit is used to represent the coverage dependence of H* adsorption. In developing these fits, we insert a data point at the zero coverage limit ($\theta = 0$) equal to that computed at $\theta = 1/9$ ML. The use of small unit cells limits the structure of adsorbates to highly ordered overlayers, likely missing the lowest energy configuration in many cases. We omit data points at a lower coverage that are less favorable than their higher coverage counterparts, as these coverages could simply segregate to higher coverage regions with bare patches. This analysis therefore only provides a first order approximation to the surface coverage dependence. The approach is adopted to suggest that the competition between CO* and H* impacts HC formation during CO_2 ER, but is approximate in neglecting the multitude of adsorbate structures that could occur. The best fit equations are derived from the DFT-computed coverage dependent free energies of CO* formation (third-order polynomial fit) $\Delta G_{rxn}^{CO^*}[\theta,U]$ and H* adsorption (linear fit) $\Delta G_{ads}^{\mathrm{H}^*}[\theta,U]$ on the metal surfaces.

The best fit coefficients for the coverage dependent terms in the Equations (S 1) and (S 2) are independent of potential. The last coefficient, which is independent of coverage, reflects the variation in $\Delta G[\theta]$ with potential. For each series of $\Delta G[U,\theta]$ the corresponding equilibrium

constant $K[U,\theta]$ is calculated and the relative surface coverage of H* and CO* are solved numerically at each value of U using Equations 6-8.

$$\Delta G_{ads}^{H^*}[\theta,U] = X[\theta] + Y\ eU \quad \textbf{(S 1)}$$

$$\Delta G_{rxn}^{CO^*}[\theta,U] = A[\theta^3] + B[\theta^2] + C[\theta] + D\ (2eU) \quad \textbf{(S 2)}$$

	A[$\theta_{CO^*}^3$]	B[$\theta_{CO^*}^2$]	C[θ_{CO^*}]	D	X[θ_{H^*}]	Y
Au (111)	−0.762	1.861	−0.403	0.366	0.143	0.768
Pt (111)	1.349	−0.590	0.502	1.874	0.151	1.716
Cu (111)	−0.413	2.060	−0.562	0.962	0.110	1.474
Ni (111)	0.451	1.311	−0.356	1.980	0.013	2.060
Co (0001)	1.360	−0.328	0.081	1.711	0.129	1.994

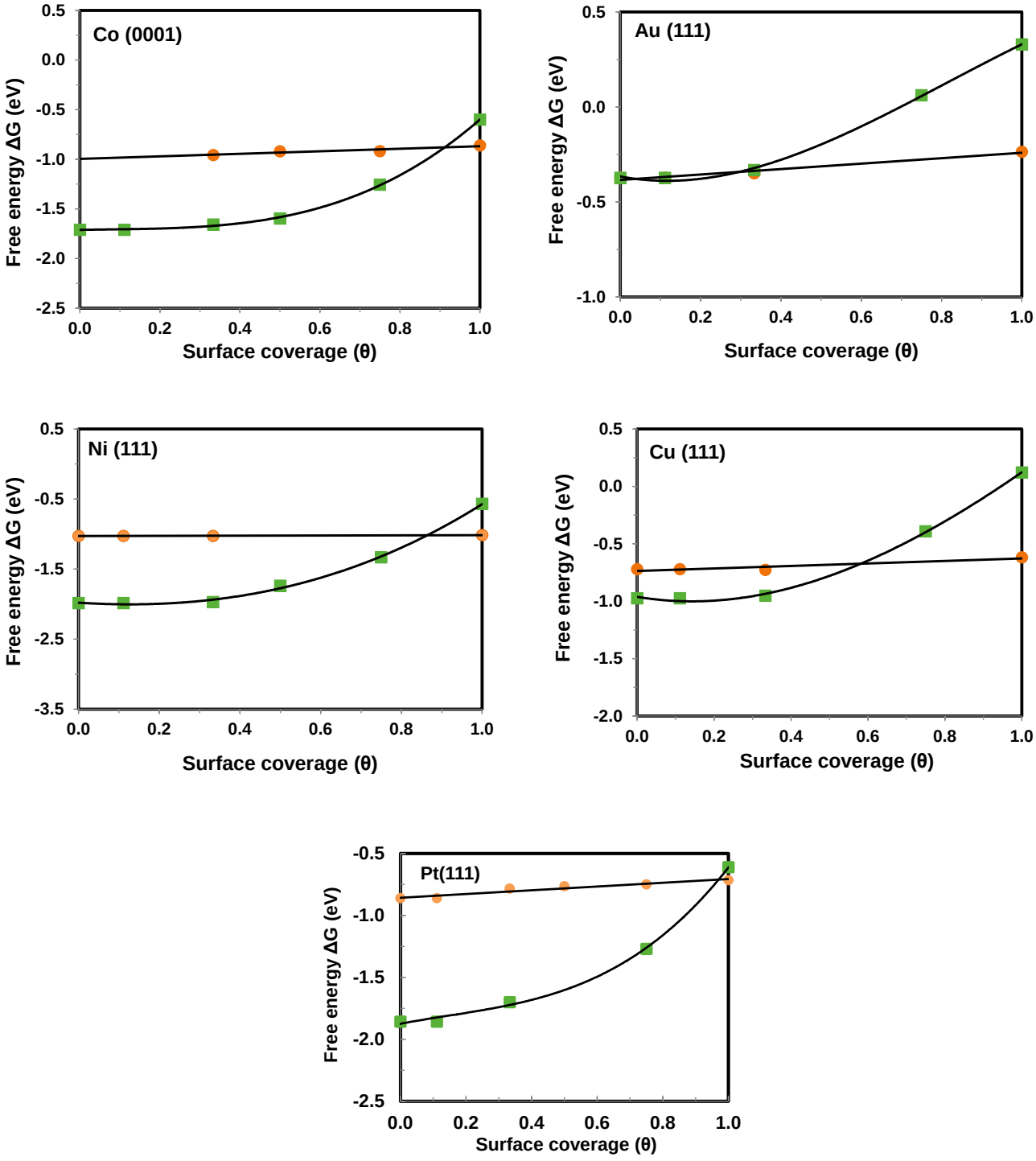

Figure S 3. Variable coverage model of H* (● orange) and CO* (■ green) on metal surfaces depicting the coverage dependent free energies at U = −0.5 V-RHE.

The equilibrium coverage $\theta_{des}^{CO^*}[U^0]$ for CO* desorption can be calculated using the equilibrium constant for CO* adsorption from gas-phase CO as follows,

$$CO_{(g)} + * \rightarrow CO^* \quad \textbf{(S 3)}$$

$$K^{CO^*}[U^0,\theta] = \frac{\theta_{des}^{CO^*}[U^0]}{\theta^*[U^0]\, p_{CO_{(g)}}} \quad \textbf{(S 4)}$$

The equilibrium coverages were determined at T = 298 K and a wide range of CO gas-phase pressures $0.001 < p_{CO_{(g)}} < 1000$ mbar. The results indicate that the $\theta_{des}^{CO^*}[U^0]$ on Cu (111) varied between 0.47 and 0.72 ML which was still less than $\theta_{des}^{CO^*}[U^0] \sim 0.998\,\text{ML}$ on Pt (111), Ni (111) and Co (0001) surfaces at different pressures. The $\theta_{des}^{CO^*}[U^0]$ values on Au (111) were very low and varied between 0.001 and 0.005 ML. For convenience, the critical equilibrium coverage value of CO* desorption was evaluated at 1 mbar pressure and 298 K temperature.

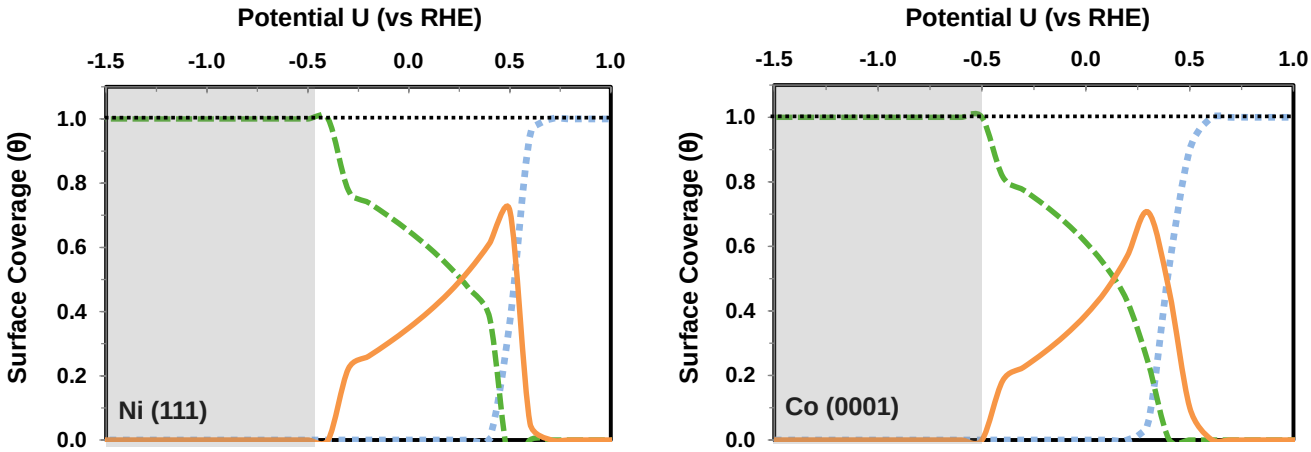

Figure S 4. Variations in surface coverage of H* (— smooth), CO* (- - dashed) and vacant sites (··· dotted) on the metal surface as a function of potential. The black dotted line (···) denotes the equilibrium coverage limit $\theta_{des}^{CO^*}[U^0]$ for CO* desorption to $CO_{(g)}$ at 1 mbar pressure and 298 K. The gray region (▮) indicates the potential range (U = −0.5 to −1.5 V) at which CO_2 ER is relevant.

4. Co-adsorption effects between H and CO on Pt (111)

The model described earlier in section 3 to calculate the potential dependent surface coverage (θ [U]) assumes no interactions between H* and CO* on the surface. To address the effect of adsorbate-adsorbate interactions on the potential-dependent relative coverages of H* and CO*, the model was modified to include co-adsorption effects between H* and CO* on Pt (111). Co-adsorption effects on Pt (111) were examined using DFT to compute the binding energy of H* and CO* at variable coverages in a 3×3 unit cell. Because the high number of possible θ_H and θ_{CO} combinations can quickly escalate the complexity of studying co-adsorption, the effect of CO* coverage on the H* binding energy and vice-versa was decoupled. The binding energy trends (calculated using Equations (S5)-(S7)) were examined within the following framework:

i. Binding energy of H* at variable coverage at fixed low ($1/9^{th}$ ML) CO* coverage− $BE_{H*}[\ \theta_H, \theta_{CO\ =\ 1/9^{th}\ ML}]$ (Refer to Equation (S 5))

ii. Binding energy of H* at variable coverage at fixed medium ($1/3^{rd}$ ML) CO* coverage− $BE_{H*}[\ \theta_H, \theta_{CO\ =\ 1/3^{rd}\ ML}]$ (Refer to Equation (S 6))

iii. Binding energy of CO* at variable coverage at fixed medium ($1/3^{rd}$ ML) H* coverage− $BE_{CO*}[\ \theta_{CO}, \theta_{H\ =\ 1/3^{rd}\ ML}]$ (Refer to Equation (S 7))

$$BE_{H^*}[\theta_{H^*}, \theta_{CO^*=1/9}] = \frac{E^{DFT}_{(CO+H)^*}[\theta_{H^*}, \theta_{CO^*} = \frac{1}{9}] - E^{DFT}_{CO^*}[\theta_{CO^*} = \frac{1}{9}] - n_H E^{DFT}_H}{n_H} \quad \textbf{(S 5)}$$

$$BE_{H^*}[\theta_{H^*}, \theta_{CO^*=1/3}] = \frac{E^{DFT}_{(CO+H)^*}[\theta_{H^*}, \theta_{CO^*} = \frac{1}{3}] - E^{DFT}_{CO^*}[\theta_{CO^*} = \frac{1}{3}] - n_H E^{DFT}_H}{n_H} \quad \textbf{(S 6)}$$

$$BE_{CO^*}[\theta_{H^*=1/3}, \theta_{CO^*}] = \frac{E^{DFT}_{(CO+H)^*}[\theta_{H^*} = \frac{1}{3}, \theta_{CO^*}] - E^{DFT}_{H^*}[\theta_{H^*} = \frac{1}{3}] - n_{CO} E^{DFT}_C - n_{CO} E^{DFT}_O}{n_{CO}} \quad \textbf{(S 7)}$$

where n_H and n_{CO} denote the total number of H and CO species bound to the surface. The binding energy trends for the co-adsorbed species are shown in Figure S 5. The binding energy trends without co-adsorption (BE_{H^*} [θ_H] and BE_{CO^*} [θ_{CO}]) are included for comparison. The figure shows that the binding energy of H* or CO* progressively weakens when the coverage of the co-adsorbate is systematically increased. The binding of H* to the Pt (111) surface is significantly affected by the co-adsorbed CO* coverage. The binding of CO* is relatively less affected by the presence of co-adsorbed H* up to a coverage of 1/3rd ML. To quantify the extent of weaker binding due to co-adsorption, we calculate the average shift in the binding energy trend relative to the same of non-co-adsorbed systems (BE_{H^*} *[θ_H]* and BE_{CO^*} *[θ_{CO}]*). This is computed using the BE best fit coefficients presented below Figure S 5. Our calculations predict that on average, CO* binds weaker to Pt (111) by 0.095 eV when H* is co-adsorbed up to θ_H~1/3 ML. On average, the H* binding weakens by 0.464 eV when CO* is co-adsorbed on the Pt (111) surface between $1/9 < \theta_{CO} < 1/3$ ML.

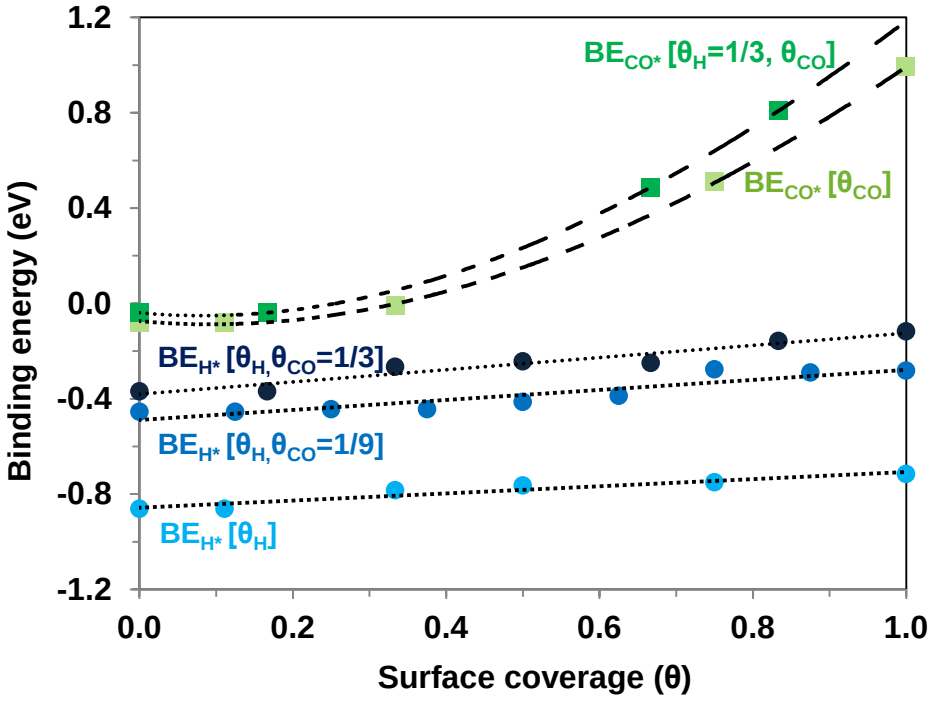

BE trend	A[θ^3]	B[θ^2]	C[θ]	D
BE$_{H*}$ [θ$_H$]	–	–	0.151	−0.857
BE$_{H*}$ [θ$_H$,θ$_{CO}$=1/9]	–	–	0.210	−0.489
BE$_{H*}$ [θ$_H$,θ$_{CO}$=1/3]	–	–	0.256	−0.381
BE$_{CO*}$ [θ$_{CO}$]	−0.251	1.610	−0.292	−0.074
BE$_{CO*}$ [θ$_H$=1/3, θ$_{CO}$]	−0.329	1.854	−0.299	−0.039

Figure S 5. Surface coverage dependent binding energy (BE) trends of co-adsorbed H* and CO* species on Pt (111). The corresponding constants for the BE trends are provided below the figure.

To evaluate the effect of co-adsorption, reflected in the weaker binding of adsorbates to the metal surface, on the potential-dependent relative coverage of H* and CO* (see Figure S 4), Equations (S 1) and (S 2) are modified to include a coverage dependent “energy penalty” term that accounts for weaker binding due to co-adsorption. These equations are re-written as follows:

$$\Delta G_{ads}^{H^*}[\theta_{H^*}, \theta_{CO^*}, U] = X[\theta_{H^*}] + Y\ eU - M\ \theta_{CO^*} \quad \textbf{(S 8)}$$

$$\Delta G_{rxn}^{CO^*}[\theta_{H^*}, \theta_{CO^*}, U] = A[\theta_{CO^*}{}^3] + B[\theta_{CO^*}{}^2] + C[\theta_{CO^*}] + D\ (2eU) - \mathrm{N}\ \theta_{H^*} \quad \textbf{(S 9)}$$

where M = 0.464 eV and N = 0.095 eV, the average energy penalty computed from the BE trends shown in Figure S 5. For each series of $\Delta G[U, \theta]$ the corresponding equilibrium constant $K[U, \theta]$ is calculated and the relative surface coverage of H* and CO* are solved numerically at each value of U using Equations 6-8. The effect of co-adsorption on the potential-dependent surface coverage of H* and CO* on Pt (111) is shown in Figure S 6 . The results are largely unchanged within the CO_2 ER active region of −1.50 < U < −0.50 V-RHE with CO* blocking access to H* on the Pt (111) surface. The effect of co-adsorption is more pronounced in the mixed coverage region at −0.50 < U > 0.50 V-RHE wherein the feasibility of H* adsorption is delayed to U ~ 0 V-RHE (relative to U ~ 0.50 V-RHE) due to the presence of co-adsorbed CO. Weaker binding contributes to narrowing the potential window within which H* adsorption is viable and resistant to the competing effects of CO* formation. Because the co-adsorbed effect on CO* binding is less significant, the relative coverage of CO* via CO* formation remains mostly unaffected in the presence of co-adsorbed H*. While co-adsorption of H* and CO* was only addressed on the Pt (111) surface, we postulate that the nature of the BE trends will be similar on other metals and will vary the relative surface coverage of H* and CO* in the mixed coverage region between −0.50 < U > 0.50 V-RHE. The results and conclusions drawn within the CO_2 ER potential region− that a high CO* coverage limits H* adsorption, remain unchanged.

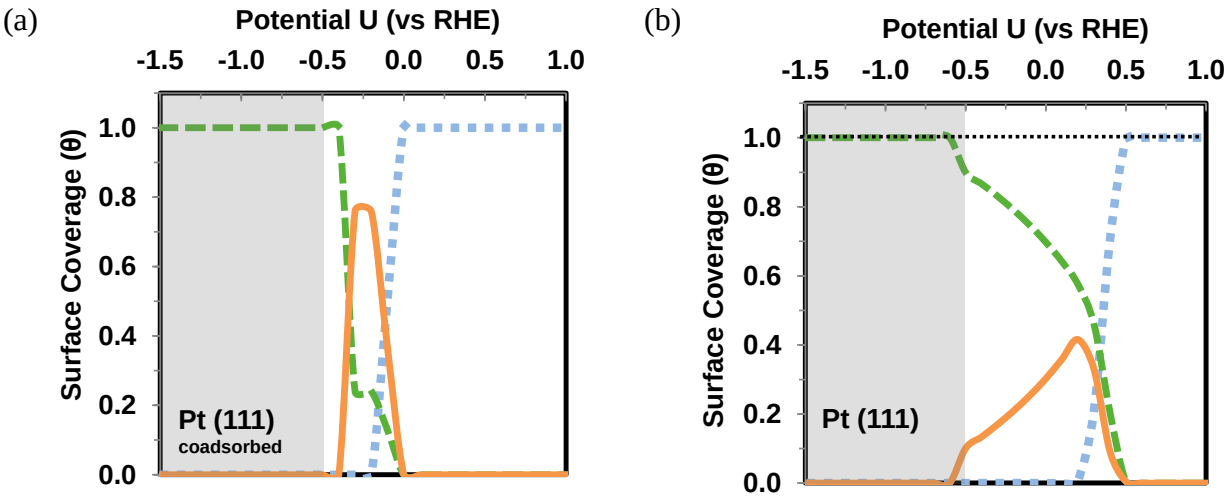

Figure S 6. Variations in surface coverage of H* (— smooth), CO* (- - dashed) and vacant sites (··· dotted) on the Pt (111) surface as a function of potential with (a) co-adsorption and (b) without co-adsorption interactions considered. The gray region (▮) indicates the potential range (U = −0.5 to −1.5 V) at which CO_2 ER is relevant.